IVYSPRING INTERNATIONAL PUBLISHER

Theranostics

2016; 6(5): 688-697. doi: 10.7150/thno.14555

Research Paper

A Phosphorus Phthalocyanine Formulation with Intense Absorbance at 1000 nm for Deep Optical Imaging

Yang Zhou[1,2*], Depeng Wang[2*], Yumiao Zhang[2,3], Upendra Chitgupi[2], Jumin Geng[2], Yuehang Wang[2], Yuzhen Zhang[4], Timothy R. Cook[4], Jun Xia[2]✉ and Jonathan F. Lovell[2, 3]✉

1. College of Chemistry, Chemical Engineering and Materials Science, Collaborative Innovation Center of Functionalized Probes for Chemical Imaging in Universities of Shandong, Key Laboratory of Molecular and Nano Probes, Ministry of Education, Shandong Provincial Key Laboratory of Clean Production of Fine Chemicals, Shandong Normal University, Jinan 250014, P.R. China.
2. Department of Biomedical Engineering, University at Buffalo, State University of New York, Buffalo, NY 14260, USA.
3. Department of Chemical and Biological Engineering, University at Buffalo, State University of New York, Buffalo, NY 14260, USA.
4. Department of Chemistry, University at Buffalo, State University of New York, Buffalo, NY 14260, USA.

* These authors contributed equally.

✉ Corresponding authors: jflovell@buffalo.edu; junxia@buffalo.edu.

Received: 2015.11.29; Accepted: 2016.02.12; Published: 2016.03.11

Abstract

Although photoacoustic computed tomography (PACT) operates with high spatial resolution in biological tissues deeper than other optical modalities, light scattering is a limiting factor. The use of longer near infrared wavelengths reduces scattering. Recently, the rational design of a stable phosphorus phthalocyanine (P-Pc) with a long wavelength absorption band beyond 1000 nm has been reported. Here, we show that when dissolved in liquid surfactants, P-Pc can give rise to formulations with absorbance of greater than 1000 (calculated for a 1 cm path length) at wavelengths beyond 1000 nm. Using the broadly accessible Nd:YAG pulse laser emission output of 1064 nm, P-Pc could be imaged through 11.6 cm of chicken breast with PACT. P-Pc accumulated passively in tumors following intravenous injection in mice as observed by PACT. Following oral administration, P-Pc passed through the intestine harmlessly, and PACT could be used to non-invasively observe intestine function. When the contrast agent placed under the arm of a healthy adult human, a PACT transducer on the top of the arm could readily detect P-Pc through the entire 5 cm limb. Thus, the approach of using contrast media with extreme absorption at 1064 nm readily enables high quality optical imaging in vitro and in vivo in humans at exceptional depths.

Key words: photoacoustic computed tomography

Introduction

Photoacoustic (PA) computed tomography (PACT) has emerged as a promising biomedical imaging modality that combines optical and ultrasound modalities to achieve improved resolution deep in tissues [1]. Based on the endogenous optical contrast of blood, PACT has been demonstrated preclinically for a range of applications including imaging of brain function, tumor vascularization and drug delivery and efficacy [2-5]. Photoacoustic contrast agents have been extensively developed and evaluated, largely in preclinical settings [6, 7]. Amongst others, these include carbon nanotubes [8], gold nanoparticles [9], virus-mimicking particles [10], organic particles [11, 12] and hybrids [13] that enable multimodal imaging [14-16]. Photoacoustic probes capable of molecular imaging of cell-surface receptors [17], proteolytic activity [18], reactive oxygen species [19] and pH have also been developed recently.

However, translating PACT into clinical applications remains challenging, due to limited penetration depth. The deepest PACT depth reported to date was 8.4 cm, as demonstrated in vitro in chicken breast tissue [20]. However, the light intensity used in that experiment was close to the ANSI safety limit, leaving

little room for further improvements in penetration depth by simply increasing the light fluence. For human imaging, PACT breast scanners have shown promising vascular images, but penetration depth was limited and not quantified [21]. Compared to other optical tomography modalities, photon-based detectors (as opposed to the ultrasonic transducer detectors used in PACT) have severely impaired light penetration depth due to light scattering and two-way light propagation. For instance, diffuse optical tomography has been reported up to 6 cm in breast, but with poor depth-to-resolution ratio (~5), which corresponds to a 1.2 cm spatial resolution, which is not suitable for imaging applications [22]. In comparison, PACT depth-to-resolution ratio is close to 200 [23].

In highly scattering media such as animal tissue, near infrared (NIR) light exhibits reduced scattering at longer wavelengths [24]. 1064 nm has been proposed as an appealing wavelength for PACT contrast agents since there are few endogenous absorbers in tissue besides water, and this is the output wavelength of the common Nd:YAG laser [25]. Most applications in PACT make use of a Nd:YAG laser coupled with additional photonic crystals or dyes to achieve upconversion to various shorter wavelengths. Direct use of 1064 nm pulses could lead to miniaturized PACT systems with greater power [26]. Additionally, human safety limits for laser outputs at 1064 nm are permissive of higher energies compared to shorter wavelengths. Several photoacoustic contrast agents have been proposed for 1064 nm laser excitation including copper sulfide nanoparticles [27], gold nanorods [28] and nanorod-containing perfluorocarbon droplets [29].

Phthalocyanines (Pcs) are hydrophobic chromophores with delocalized macrocycle electrons, strong NIR absorption, diverse metal coordination capacity and good stability (e.g. some Pcs have been shown to be stable at temperatures as high as 900 °C) [30, 31]. They have a history for use a theranostic agents, dating back over 60 years [32]. Much research emphasis has been placed on their applications in molecular photovoltaics [33], thin-film electronics [34], sensors [35], photosensitizers for photodynamic therapy [36, 37], molecular magnets [38], nonlinear optical materials [39], and catalysts [40]. There have also been several examples of Pcs being used for photoacoustic imaging.[41-43].

We previously reported that functional intestinal imaging and multicolor lymph node mapping is possible using nanoformulated Pcs and naphthalocyanines [44, 45]. Highly hydrophobic dyes induced the formation of frozen micelles which enabled the subsequent removal of unincorporated surfactant, leaving behind a concentrated nanoparticle solution that could achieve absorbance greater than 1000. The longest wavelength dye used had a peak absorption at 860 nm.

Recently, Kobayashi's group has pioneered the rational design of stable, far NIR Pcs with optical absorption bands at wavelengths greater than 1000 nm [46, 47]. These unique Pcs feature a central, chelated, electron deficient Group 15 element (e.g. P, As, Sb) and outer benzene groups functionalized with electron rich Group 16 elements (e.g. S, Se, Te). In this study, we synthesize a phosphorus Pc (P-Pc) that contains a central phosphorus and outer sulfur and demonstrate its potential to enable deep PACT in vitro and in vivo. To show the generalized synergy for P-Pc and PACT applications, tumor-bearing mice were used with intravenously administered P-Pc for tumor imaging, healthy mice were used with orally administered P-Pc for intestinal imaging, and human studies were conducted with external placement of the contrast agent across the arm to show capability for deep imaging in humans.

Results and Discussion

P-Pc formulation

The phosphorus Phthalocyanine (P-Pc) was prepared as shown in **Figure 1,** according to recent literature [46]. All steps in the synthesis had very good to excellent yields (83-95 %), with the exception of generating one of the precursors, **P2**, which was obtained with just 8 % yield. To solubilize the hydrophobic P-Pc product in a biocompatible medium, 20 mg/mL of P-Pc was dissolved in liquid surfactants including Tween 20, Tween 40, Tween 80, Cremophor EL, Pluronic F68, or edible oils including canola, olive and soy oil. Optical absorbance was assessed directly without dilution using a 10 μm path length cuvette, and values are multiplied by 1000 to determine the calculated absorbance in a 1 cm path length cuvette (**Figure 2A**). P-Pc that was dissolved in Tween and Cremophor EL had the highest absorbance of greater than 800, at a wavelength close to 1000 nm. The solution was centrifuged prior to measurement and was not cloudy, so that any light scattering contribution to the absorbance was minimal. The surfactants themselves had no background absorption at that wavelength. Pluronic F68, oils and water could not dissolve P-Pc well and produced negligible absorbance, showing these were not suitable carriers. Tween 80 (also referred to as Polysorbate 80), was selected for further studies since it has been approved by the FDA for oral consumption and is a common food and cosmetic additive. The absorbance spectrum P-Pc dye in Tween 80 exhibited an absorption peak at 997 nm, which was blue shifted by 45 nm compared to P-Pc in

chloroform (**Figure 2B**). This is likely due to different packing and electron interactions of concentrated P-Pc molecules in the Tween surfactant, and this phenomenon has been shown to affect Pc optical properties [48]. The absorbance of P-Pc at 1000 nm was also measured following dilution into water with a standard 1 cm path length cuvette (**Figure S1** in the Supporting Information). The P-Pc absorbance at 1000 nm was approximately linear with increasing P-Pc concentrations in Tween 80.

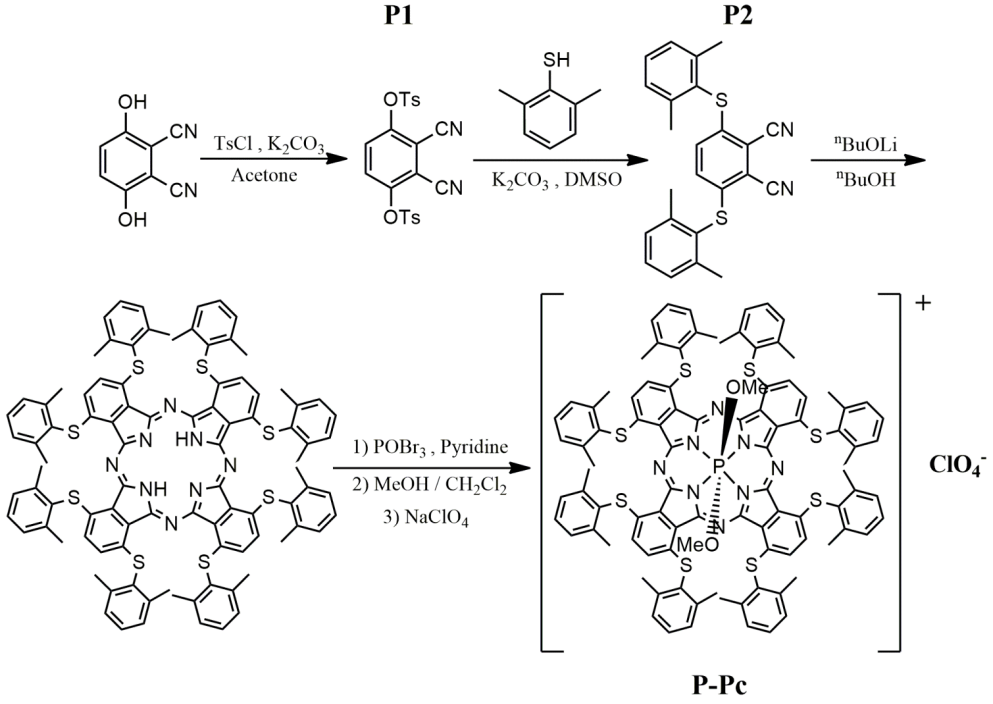

Figure 1. Synthesis of phosphorus phthalocyanine (P-Pc): [α-(2,6-dimethylphenylthio)$_8$PcP(OMe)$_2$]$^+$[ClO$_4$]$^-$

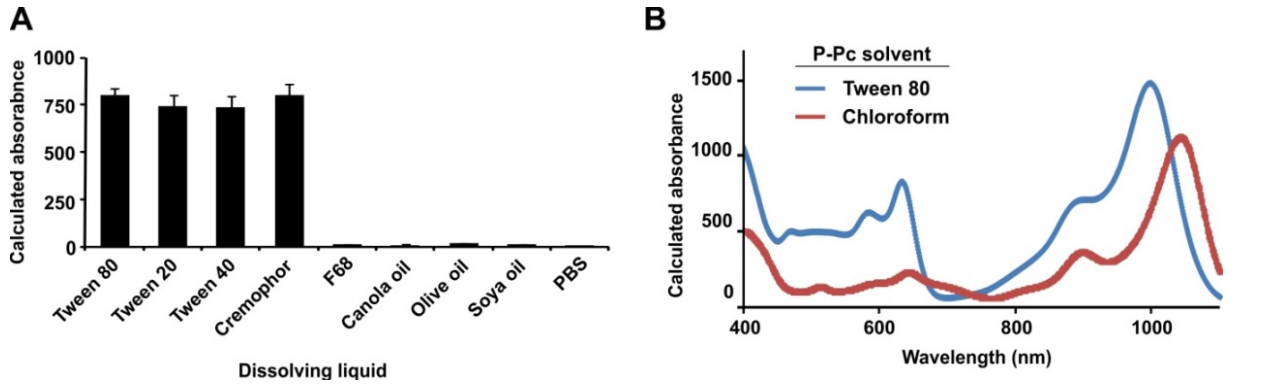

Figure 2. Absorbance of P-Pc in excipients. (A) Calculated absorbance of P-Pc at 997 nm following dissolution in the indicated liquids at 20 mg/mL P-Pc. Samples were briefly centrifuged prior to measurement in a cuvette with a 10 μm path length. Absorbance was multiplied by 1000 to produce calculated absorbance based on a 1 cm path length (mean ± s.d. for n = 3). **(B)** Calculated absorbance of 40 mg/mL P-Pc dye in Tween 80 (blue) or 20 mg/mL in chloroform (red). The Tween formulation was measured directly with a 10 μm path length cuvette. Since chloroform was not compatible with the 10 μm path length cuvette, it was diluted 1000 times into a conventional cuvette. Absorbance was multiplied by 1000 for calculated absorbance of the solution, based on a 1 cm path length.

Deep imaging in chicken breast tissue

To assess the penetration depth using PACT and P-Pc, we performed a phantom experiment with chicken breast tissue. The experiment was performed in a similar manner as a previous study [20], which to our knowledge set the current record for the deepest PACT detection depth through 8.4 cm of tissue (detecting methylene blue through chicken breast). Before the experiment, 30 mM of dye was placed in a 35 mm long Tygon tube with a 5 mm inner diameter. This concentration was the same as the one used in the previous depth record [20]. To prevent leakage, both ends of the tube were tied and sealed with epoxy glue. The tube was placed in a 2 L glass breaker whose bottom was covered with 2.5 cm thick chicken breast tissue. As shown in **Figure 3A,** pieces of chicken breast tissue were consecutively stacked on top of the tube and the photoacoustic signal change was monitored. The tube photoacoustic signal started to be ob-

scured by noise when the tissue thickness reached approximately 12 cm (without any signal averaging). The corresponding light intensity was 56 mJ/cm^2 over the 3 cm diameter illumination region. Because averaging can improve the signal to noise ratio (SNR), we acquired 100 images at the same depth. The overlaid averaged photoacoustic and ultrasound images are shown in **Figure 3B**, where the tube is clearly visible in the color photoacoustic image. The photoacoustic signal outside the dotted frame indicated in the figure is not shown. The SNR was quantified to be 18 dB, which is higher than the 15 dB SNR previously reported with 200 times averaging [20]. The actual imaging depth in PA image was calculated to be 11.6 cm, which is close to the depth measure by a ruler (~12 cm). To ensure that no light leaked to the tube through the bottom of the beaker, we repeated the experiment with ~12 cm of chicken tissue placed both on top and beneath the tube. Again, the tube could be clearly visualized (**Figure S2 in the Supporting Information)**. We also gradually removed the tissue on top and computed the signal to noise ratio of the PA signal at different penetration depths. This data is shown in **Figure S3 in the Supporting Information**. Thus, the use of P-Pc as a contrast agent with this photoacoustic computed tomography (PACT) system improved upon the deepest reported optical imaging depth in tissue by 38%, with only half the amount of averaging. Moreover, the light intensity used was only around half of the ANSI safety limit, whereas the previous example was within 85 % of the safety limit [20]. The deeper penetration depth is mainly attributed to the high absorption of P-Pc formulation at 1064 nm, weak tissue absorption and scatter in the deep NIR, and the higher ANSI safety limit at 1064 nm. We did not perform experiments at the full ANSI safety limit. Although these experiments were in tissue phantoms, the deep detection of P-Pc through over 10 cm of biological tissue shows its potential for clinical applications that require penetration beyond a couple of centimeters.

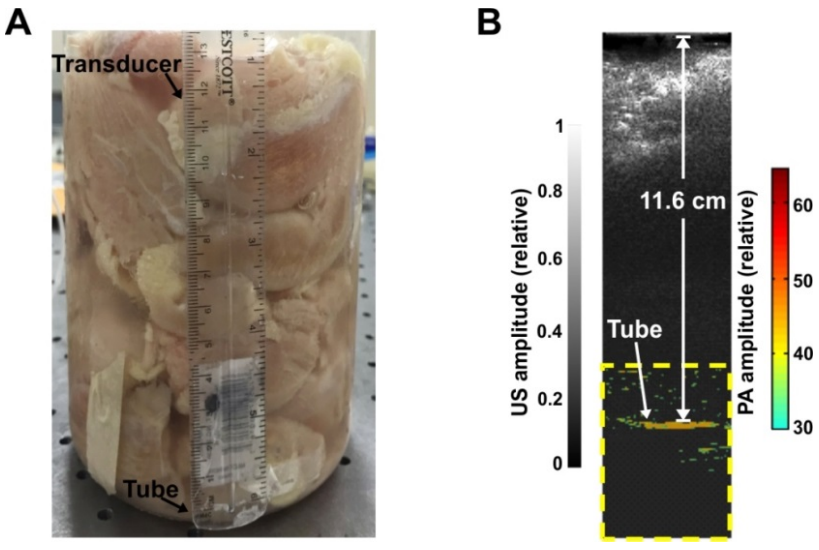

Figure 3. Detection of P-Pc through 11.6 cm of tissue. (**A**) Photograph of the sample setup with chicken breast stacked on top of a tube containing the P-Pc formulation. (**B**) Overlaid photoacoustic (color, within the dashed box) and ultrasound (gray) images of the tube at 11.6 cm depth.

Tumor Imaging

To investigate P-Pc for tumor imaging, nude mice bearing pancreatic MIA PaCa-2 xenografts grown in the left groin were imaged. For all experiments, the light intensity was controlled on the animal skin to be approximately 8.5 mJ/cm^2, over a 3 cm diameter region. This energy is less than a tenth of the permissible ANSI safety limit. The scanning geometry is shown in **Figure 4A**. For each experiment, the animal was scanned over 20 mm along the elevation direction at a step size of 0.1 mm. At each step, one frame of ultrasound and photoacoustic images were captured using the L7-4 transducer array.

Tumors were imaged in mice with or without intravenous administration of P-Pc. To administer P-Pc, the 100 mg/mL P-Pc, Tween 80 stock solution was diluted to 25 mg/mL with pure water and mice were injected via tail vein. Mice were intravenously administered 100 µL of this diluted formulation (with a calculated absorbance at 1002 nm of 200, based on a 1 cm path length; dilution of P-Pc into water shifted peak absorbance wavelength by 5 nm). Imaging was performed 24 hours after P-Pc injection. Because we used the same light intensity for all treated mice, for better comparison, both reconstructed images were normalized with the same values. **Figure 4B** shows representative cross sections from a control mouse. Because at 1064 nm, the intrinsic optical absorption of biological molecules is negligible and water absorption is low and homogenous, the PA signals were weak and were all below the threshold used to render the superimposed image. For mice treated with P-Pc, an intense PA signal was observed in the tumors, indicating extravasation of P-Pc to the tumor, probably through the enhanced permeability and retention effect. At the 24 hour point, most of the P-Pc accumulated in the liver with modest accumulation in the tumor, but a large amount remained in circulation (**Figure S4 in Supporting Information**). In the future, exploration of targeted molecular imaging approaches would be useful to possibly improve the tumor specificity of P-Pc. The NIR P-Pc contrast in the tumor could also be explored in the future for photothermal therapy.

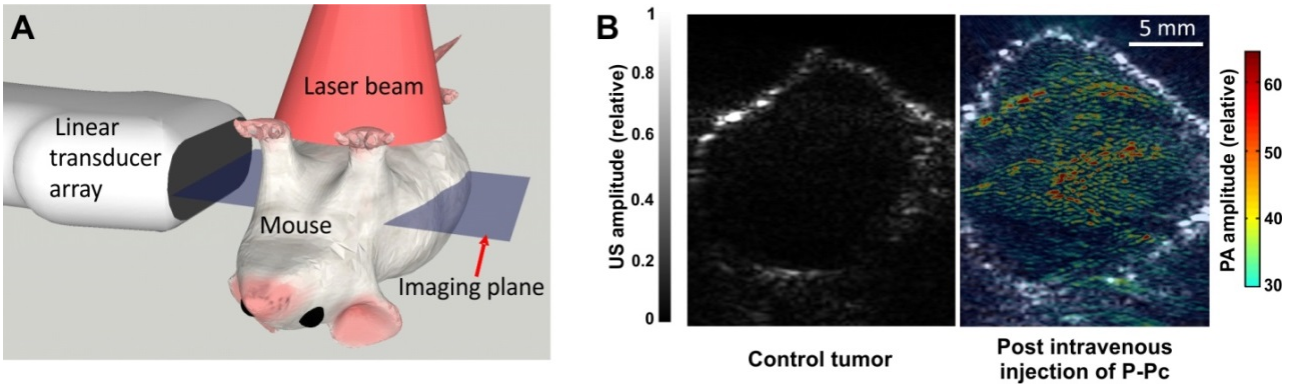

Figure 4. PACT tumor imaging using P-Pc. (A) Schematic of the PACT system and imaging geometry. (**B**) Tumor PACT imaging in untreated or mice intravenously administered P-Pc. The tumor image was obtained 24 hours after tail vein injection. Tumor images are representative for n=3 mice. PA is shown in color and US is shown in gray.

Analysis of PA signal intensities indicated that the PA contrast in the tumor was 1.9 times higher than tissues surrounding the tumor and 2.3 times higher than the signal found in the tumor of untreated control mice. This experiment shows that not only can P-Pc accumulate in tumors for PACT-based imaging, but also that P-Pc was tolerated following systemic administration to mice. In vitro, when U87 glioblastoma cells were incubated with P-Pc for 24 hours, no decrease in viability was observed relative to the Tween 80 carrier itself (**Figure S5 in the Supporting Information).** However, at higher concentrations, Tween 80 itself strongly inhibited cell viability. Although Tween 80 is used as an excipient in several injectable drugs, further toxicity testing is required to better understand the systemic effects of P-Pc and Tween 80. This underscores the advantages of previously reported approaches such as surfactant-stripping, to minimize the amount of surfactant used to solubilize hydrophobic dyes [44].

Dynamic Intestine Imaging

To assess the suitability of P-Pc as an orally administered PA agent, the stability of the P-Pc in Tween 80 was first tested in vitro in simulated gastric and intestinal fluids. The P-Pc formulation was diluted into and then dialyzed against simulated gastric fluid at 37 °C. No appreciable loss of optical absorbance was observed over 8 hours (**Figure 5A**). When the same procedure was performed using simulated intestinal fluid, less than 10 % absorbance loss was observed in 4 hours and less than 20 % absorbance loss was observed in 8 hours. This demonstrates that P-Pc had good chemical stability under harsh dialysis conditions, and also that the hydrophobic chromophore was able to form supramolecular structures that are not small enough to pass through the dialysis membrane. No change in spectral properties were observed during incubation in these conditions (**Figure S6 in the Supporting Information).** Following oral administration to mice, P-Pc was excreted and could be fully recovered from feces in less than 24 hours (**Figure 5B**). Thus, P-Pc was stable throughout the gastrointestinal tract and was not absorbed systemically. This behavior is similar to our recent report of nanoformulated Pc and naphthalocyanine dyes that were fully excreted in feces following oral administration [44]. A contrast agent that is stable in the gut and is not systemically absorbed is advantageous for intestinal imaging applications with respect to safety and signal consistency in the intestinal lumen.

P-Pc was next assessed as an intestinal contrast agent for PACT in vivo in mice. The PA scanning geometry was similar as that shown in **Figure 4A**. The L7-4 transducer was replaced with the L12-5 (38 mm) transducer, which has more elements (192 vs. 128) and better spatial resolution (axial resolution: 0.83 mm vs. 1.5 mm, lateral resolution: 0.2 mm vs. 0.3 mm). The laser intensity was controlled to be the same as in the tumor imaging experiments. Minimal background PA signals were observed in mice before administration of P-Pc. Half an hour after mice were orally administered 100 μL of 25 mg/mL P-Pc formulation (with calculated absorbance at 1002 nm of 200, based on a 1 cm path length), the mouse was imaged at a rate of 3.33 frames per second. This frame rate is sufficient to track the intestine peristalsis, which occurs approximately every two seconds in mice. To mitigate motion artifacts caused by respiration, we computed the covariance matrix of all image frames, identified ones with the largest body displacement (based on amplitudes of the eigenvector), and replaced these frames with neighboring averages. Representative frames are shown in **Figure 5C**, in which the transition of the dye within the white grids can be clearly identified. The peristaltic rate was calculated based on the average signal amplitude within a red rectangular area (**Figure 5D)**. Thirty peaks can be identified within a 60 second time window, indicating a peristaltic rate of 30 per minute, which is the expected rate in mice. For better illustration, the peristaltic rate was calculated

over time (**Figure 5E**), showing a peristaltic rate close to 30 contractions per minutes.

Trans-limb Imaging in Humans

To demonstrate the translational potential of deep PACT with highly absorbing contrast at 1064 nm, we attempted imaging through a human arm, something that to our knowledge has not yet been done with optical imaging. As ultrasound cannot propagate through bone well, the transducer and light source were directed towards the space between the ulna and radius bones. A tube containing the P-Pc formulation was placed beneath the arm of a healthy and conscious adult human, as shown in **Figure 6A**. When the arm was first imaged with the hybrid photoacoustic and PACT system, ultrasound could visualize the whole arm and no photoacoustic signal was present (**Figure 6B**). The ultrasound signal visible at the bottom of the arm corresponded to ultrasound reflection from the supporting agar gel under the arm. However, when a small tube containing P-Pc was placed under the arm, its complete shape could be unambiguously visualized with PACT through the 3.1 cm arm. The established ANSI safety limit for human exposure to the Nd:YAG laser pulse is 100 mJ/cm^2, and this pilot study a pulse of just 14 mJ/cm^2 was applied. Another volunteer with a larger arm was also imaged (**Figure 6C**). For this arm, pulse fluence was increased to 23 mJ/cm^2, which is less than a quarter of the well-established safety energy limit. The P-Pc tube was clearly detectable through the 5 cm arm. There was no bone visible in the imaging plane, because the transducer imaged in between the gap between the ulna and radius bones. Skin was not easily observed either, likely because the transducer was placed directly against it.

These data suggest that clinically relevant PACT applications such as sentinel lymph node mapping for cancer staging in deep tissues could be enabled using appropriate contrast agents with absorption beyond 1000 nm. Eventually, by localizing lymph nodes with PACT, a minimally-invasive fine needle aspiration biopsy could be performed to determine whether cancer has spread to lymph nodes, and this information could be used to guide surgical decisions whether or not to resect lymph nodes. Previously, using a shorter wavelength (667 nm), sentinel lymph node imaging in humans was reported at just over 2 cm in depth with an optimized system that was operating at 50% of the ANSI safety limit [49]. Although we did not involve injection of P-Pc into patients, contrast imaging was readily achieved through 5 cm of arm tissue, which corresponds to a less fatty and more scattering media compared to breast tissue, and at less than 25% of the ANSI safety limit.

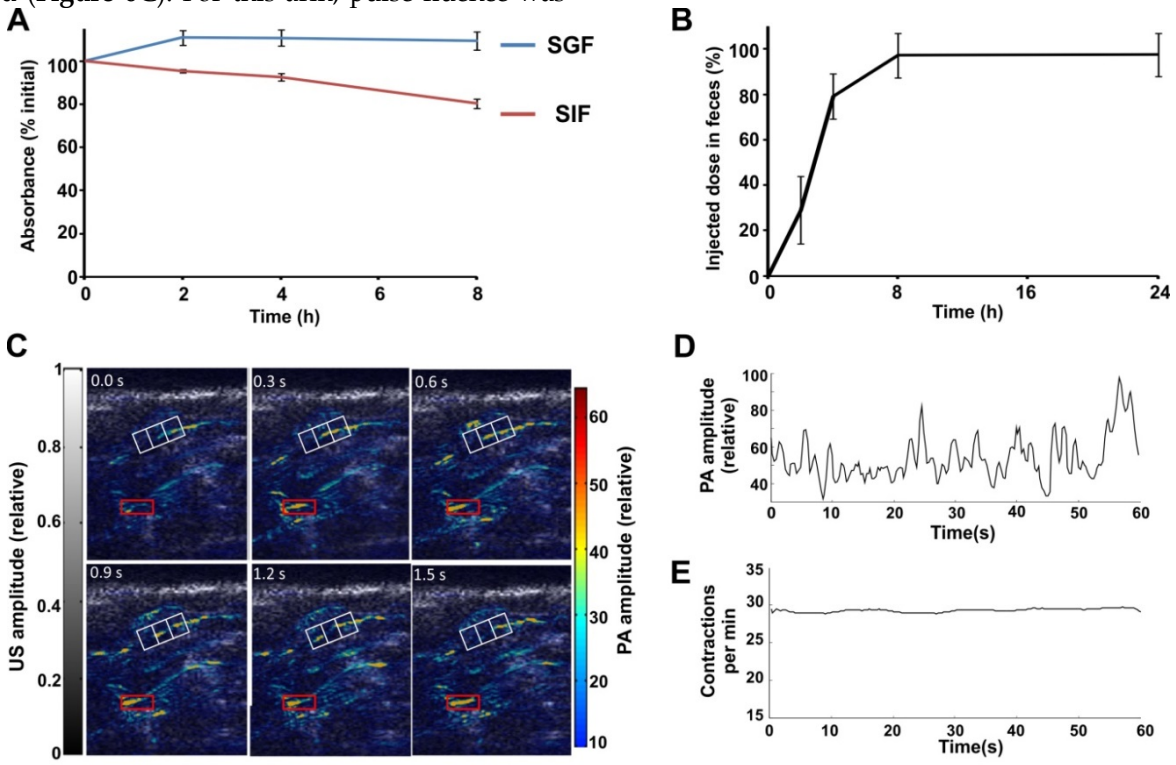

Figure 5. Suitability of P-Pc as a lumen-confined intestinal contrast agent. (A) Retained absorbance of P-Pc during dialysis against simulated gastric fluid (SGF, blue) or simulated intestinal fluid (SIF, red) at 37 °C (mean ± s.d. for n = 3). **(B)** Excretion of P-Pc in feces. Mice were gavaged with 100 µL of dye (with a calculated absorbance of 200 at 1002 nm, based on a 1 cm path length) and feces were collected and analyzed over time (mean ± s.d. for n = 3 mice). (**C**) Dye movement in the intestine. The white reference grid clearly demonstrates the movement of P-Pc in the intestine and the red box is the selected area for motion rate calculation. (**D**) Variation of photoacoustic signal within the region of interest (marked red box in C), plotted over time. (**E**) Rate of contractile motion from the same region of interest, plotted over time.

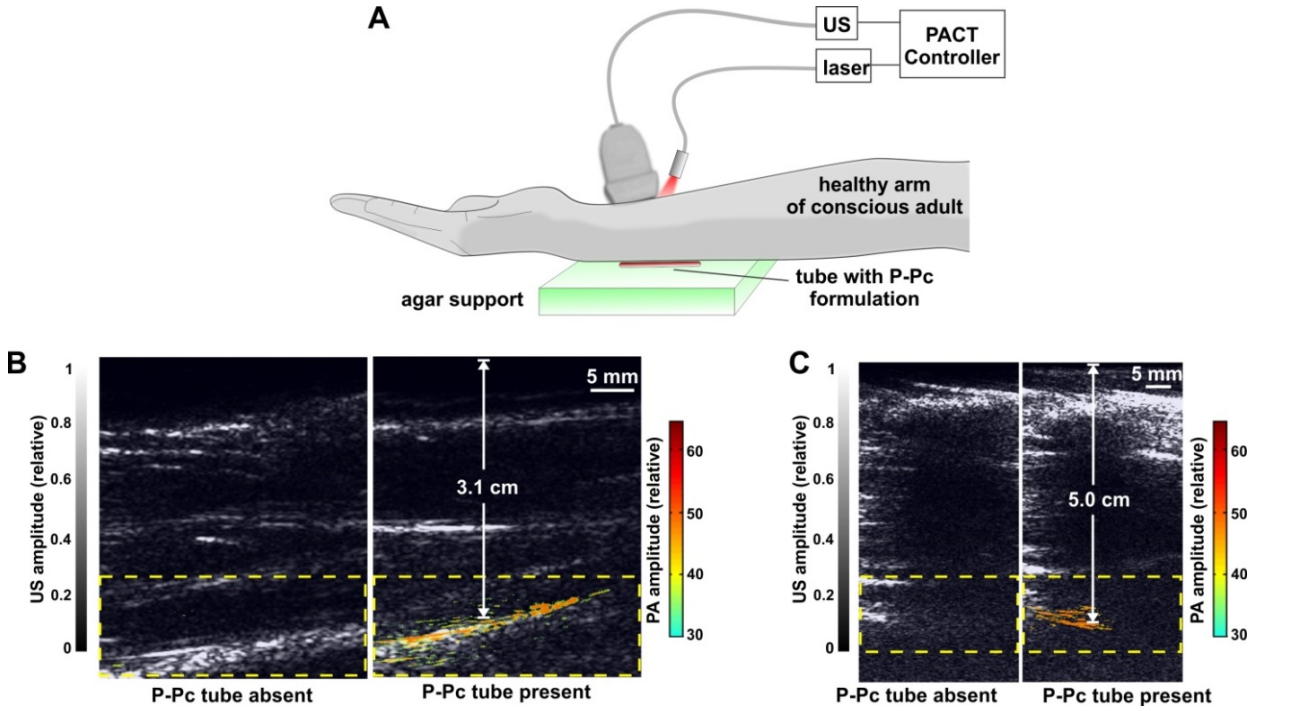

Figure 6. Trans-limb PACT of a human arm. (**A**) Experimental PACT setup. (**B, C**) Representative trans-limb PACT for 2 different adult human volunteers. Overlaid photoacoustic (color, within the dashed boxes) and ultrasound (gray) images. The PA signal of the tube was clearly visible under the arm. The signal to noise ratio was 37 dB and 32 dB in the 3.1 cm and 5.0 cm arm experiments, respectively. This distance was between the tube and the skin at the top of the arm, which was in direct contact with the transducer.

Conclusion

P-Pc is a small molecule that could readily be formulated in commonly used surfactants to produce solutions with extreme absorption beyond 1000 nm. P-Pc was used for optical imaging through 11.6 cm of chicken breast tissue, which to our knowledge represents the deepest optical biological imaging reported to date. P-Pc was tolerated in mice and proved suitable for tumor imaging following intravenous administration. Further work is required to characterize the toxicity profile of P-Pc and the Tween 80 carrier. Following oral administration, P-Pc passed harmlessly through the GI tract without entering into systemic circulation and could be used for intestinal imaging. P-Pc was imaged through an entire 5 cm arm of a healthy human adult, using an imaging geometry with both light source and detector on the top of the arm. These data show that P-Pc and other agents that are highly absorbing beyond 1000 nm can enable optical imaging with good resolution at unprecedented depths.

Materials and Methods

Materials were purchased from Sigma unless otherwise noted.

Synthesis of the Phosphorus Phthalocyanine

The phosphorus phthalocyanine (P-Pc) was prepared according to the literature as shown in **Figure 1** [46].

3,6-Bis(4′-methylphenylsulfonyloxy)phthalonitrile (P1): Precursor **P1** was prepared according reported methods [50]. In brief, p-Toluenesulfonyl chloride (5.20 g, 27 mmol) was added to a mixture of 2,3-dicyanohydroquinone (2.00 g, 12.5 mmol) and potassium carbonate (6.90 g, 50 mmol) in acetone (15 mL). The mixture was heated to reflux for 2 h, cooled to room temperature, poured into water (40 mL) and stirred for 1 h. The light brown product was filtered and oven dried to get **P1** 5.60 g (Yield 95.7 %). IR [υ_{max} / cm^{-1}]: 3432, 3239, 3085, 2243, 2226(CN), 1504, 1449, 1315, 1279, 1204, 1174, 1142, 1021, 1004, 979, 934, 847, 749, 694, 638, 614.

3,6-Bis(2,6-dimethylphenylthio)phthalonitrile (P2): P1 (2.34 g, 5 mmol) and potassium carbonate (2.80 g, 20 mmol) were added to a solution of 2,6-dimethylthiophenol (4.40 g, 30 mmol) in dimethyl sulfoxide (DMSO). After stirring for 14 h at room temperature, the reaction was quenched with water. The mixture was extracted with chloroform and washed with 5 % sodium carbonate (w/v) in water. The organic layer was dried over magnesium sulfate and concentrated in *vacuo*. The product was purified by silica gel column chromatography ($CHCl_3$) followed by recrystallization with methanol. **P2** was obtained (160 mg, 8.0 %) as a pale yellow powder. 500 MHz ^{1}H NMR ($CDCl_3$): δ = 7.25 (d, 2H), 7.17 (d, 4H),

6.40 (s, 2H), 2.36 (s, 12H).

α-(2,6-dimethylphenylthio)$_8$PcH$_2$: P2 (160 mg, 0.4 mmol) was added to a solution of lithium (28 mg, 4.0 mmol) in 2 mL of n-butanol and heated under reflux for 2 h. The mixture was purified by alumina gel column chromatography ($CHCl_3$). The free-base phthalocyanines **α-(2,6-dimethylphenylthio)$_8$PcH$_2$** was obtained (133 mg, 83 %) as a dark red powder. ESI mass calculated for $C_{96}H_{82}N_8S_8$ $[M]^+$: 1602.4, Found: 1603.7

[α-(2,6-dimethylphenylthio)$_8$PcP(OMe)$_2$]$^+$[ClO$_4$]$^-$ (P-Pc): Phosphorus oxybromide (1.5 g, excess) was added a solution of **α-(2,6-dimethylphenylthio)$_8$PcH$_2$** (133 mg, 83 μmol) in 2 mL of pyridine and stirred for 30 min at room temperature. After the solvent was removed in *vacuo*, the residue was dissolved in a solution of dichloromethane / methanol (50/50, v/v) and stirred for 30 min at room temperature. The organic layer was collected, washed with water, and solvent was removed to yield a dark green product (phosphorus Pc). The resulting solid was dissolved in dichloromethane, then sodium perclorate (41.5 mg, 340 μmol) was added. After the mixture was stirred for 12 h at room temperature, solvent was removed, and the residue was recrystallized from dichloromethane / n-hexane. **P-Pc** was obtained (120 mg, 85 %) as a dark green powder. 400 MHz ^{1}H NMR (CD_2Cl_2): δ = 7.35-7.33 (m, 8H), 7.30-7.28 (m, 16H), 6.88 (s, 8H), 2.52 (s, 48H), 0.31 (d, 6H, ^3JP_H = 26.8 Hz). ESI mass calculated for $C_{98}H_{86}N_8O_2PS_8[M\text{-}ClO_4]^+$: 1693.4, Found: 1693.7. Extinction coefficients ($M^{-1}cm^{-1}$) were measured in various solvents at the following peak absorption wavelengths: (chloroform: 1.1×10^5 at 1042 nm); (methylene chloride: 1.1×10^5 at 1029 nm); (dimethyl sulfoxide: 6.4×10^4 at 998 nm); (tetrahydrofuran: 9.7×10^4 at 1011 nm).

P-Pc formulation and characterization

10 mg P-Pc was weighed and dissolved in 100 μL of liquid surfactant, followed by sonication for 30 minutes. For oil-based dissolution, olive, canola and soy oils were obtained from a local grocery store. Samples were briefly centrifuged prior to absorbance measurement with a Lambda 35 UV/VIS spectrophotometer (Perkin Elmer) using cuvettes with a 10 μm path length (Starna # 20/O-Q-0.01). For further studies, the surfactant-dissolved P-Pc was then diluted 1:4 in water with vortexing and sonication to get the P-Pc formulation. Following dilution, absorbance was measured with cuvettes with 1 cm path length. To assess the stability of the P-Pc dye in simulated gastric fluid or simulated intestinal fluid, concentrated P-Pc in surfactant (Tween 80) was diluted into the fluids so that the absorbance was close to 1, then dialysed at 37°C against simulated gastric fluid (Ricca, #7108-32) with added pepsin and pancreatin-containing simulated intestinal fluid (Ricca #7109-32). The retention of the P-Pc dye was calculated by the ratio of absorbance to the original value.

For cell viability, U87 cells (ATTC) cells were grown in Dulbecco's modified Eagle's medium supplemented with 10% fetal bovine serum (FBS) and 1% penicillin-streptomycin at 5% CO_2 in a humidified atmosphere. Cells were seeded at a density of 1×10^4/well and incubated at 37 °C in for 24 hours. Cells were rinsed with phosphate buffered saline (PBS) and P-Pc or the Tween 80 carrier alone was added to the wells containing DMEM with serum and incubated at 37 °C for 24 hours. P-Pc containing media was replaced fresh media after washing the cells with PBS. 24 hours later the XTT assay was performed. 100 μL of PBS containing 50 μg/mL of XTT (2,3-Bis(2-Methoxy-4-Nitro-5-Sulfophenyl)-2H-Tetrazolium-5-Carboxanilide) and 60 μg/mL of PMS (N-methyl dibenzopyrazine methyl sulfate) was added to each well and incubated for 2 hours. Background (read at 630 nm) was subtracted from the absorbance read at 450 nm. Cell viability was determined by comparing the absorbance of the wells treated with dye to untreated wells. All measurements were made in triplicate.

Linear-array-based Photoacoustic Computed Tomography (PACT)

The 1064 nm output from an Nd:YAG laser was routed to the imaging region through a 1.4 cm diameter fiber bundle. The maximum light intensities at the skin surface varied from 8.5 mJ/cm^2 to 56 mJ/cm^2 in different experiments, but were all below the American National Standards Institute (ANSI) safety limit (100 mJ/cm^2) at 1064 nm. Photoacoutic (PA) signals were detected either with a 128-element linear transducer array (5 MHz central frequency ATL/Philips L7-4) for chicken tissue and tumor targeting experiments, or with a 192 element linear transducer array (9 MHz central frequency, ATL/Philips L12-5 38mm width) for intestine experiments. PA signals received by the transducer array were multiplexed and digitized by a 64-channel ultrasound data acquisition system (Vantage, Verasonics). The raw channel data were reconstructed and displayed in real-time using the universal back-projection algorithm [51].

Animal experiments

Animal experiments were performed in accordance with the University at Buffalo Institutional Animal Care and Use Committee. For tumor imaging studies, 5×10^6 MIA Paca-2 cells (obtained from ATCC) were injected in female nude mice mice (5 weeks, Jackson Labs, #007850) and were allowed to grow.

The P-Pc formulation (25 mg/mL in 25% Tween 80), was intravenously administered via tail vein (100 μL of solution with an absorption at 1002 nm of 200). For intestinal studies, female BALB/c mice (Harlan) were held without food overnight with free access to water. After gavaging 100 μL of P-Pc (absorption at 1002 nm of 200), mice were transferred to metabolic cages, and feces were collected. Peristaltic rate was calculated by dividing the peak number by the peak time in Fig. 5D. For the determination of recovery, the absorbance of serum samples was measured directly. Feces or tissues were dissolved in 2 ml of chloroform and were disrupted with a Tissue Tearor homogenizer until they were fully homogenized, and then absorbance was assessed. For PACT intestinal imaging, female nude mice were used due to their lack of hair.

Human experiments

Conducted experiments were reviewed by the University at Buffalo IRB committee. The array used in the experiment was a 128-element linear transducer array (5 MHz central frequency ATL/Philips L7-4), which is the same as we used in the tumor and chicken breast tissue experiments. 30 mM of P-Pc was filled in a 35 mm long Tygon tube with a 5.0 mm inner diameter (the same tube was also used in the chicken breast tissue experiment). The tube was placed on top of a piece of intralipid and agar gel mixed phantom (4 cm in thickness), and the arm was put on top of the tube. Ultrasound gel was used in the experiment as a coupling medium. Gel was placed both under (coupling tube and arm) and on top of the arm (coupling arm and transducer). The 1064 nm output from an Nd:YAG laser was routed to the arm through a 1.4 cm diameter fiber bundle. The maximum light intensities at the skin surface was 23 mJ/cm^2.

Abbreviations

P-Pc: Phosphorus Phthalocyanine; PACT: Photoacoustic computed tomography; US: Ultrasound.

Supplementary Material

Supplementary Figures.
http://www.thno.org/v06p0688s1.pdf

Acknowledgements

The authors thank the Shandong Provincial Education Association for International Exchanges. This work was supported by the National Institutes of Health (R01EB017270, DP5OD017898 and R21EY026411), University at Buffalo Startup Funding, and the National Natural Science Foundation of China (No. 21401118).

Competing Interests

The authors have declared no competing interest.

References

1. Kim C, Favazza C, Wang LV. In Vivo Photoacoustic Tomography of Chemicals: High-Resolution Functional and Molecular Optical Imaging at New Depths. Chem Rev. 2010; 110: 2756-82.
2. Wang X, Pang Y, Ku G, Xie X, Stoica G, Wang LV. Noninvasive laser-induced photoacoustic tomography for structural and functional in vivo imaging of the brain. Nat Biotech. 2003; 21: 803-6.
3. Siphanto RI, Thumma KK, Kolkman RGM, Leeuwen TGv, Mul FFMd, Neck JWv, et al. Serial noninvasive photoacoustic imaging of neovascularization in tumor angiogenesis. Opt Express. 2005; 13: 89-95.
4. Xia J, Kim C, Lovell JF. Opportunities for Photoacoustic-Guided Drug Delivery. Curr Drug Targets. 2015; 16: 571-81.
5. Nie L, Huang P, Li W, Yan X, Jin A, Wang Z, et al. Early-stage imaging of nanocarrier-enhanced chemotherapy response in living subjects by scalable photoacoustic microscopy. ACS Nano. 2014; 8: 12141-50.
6. Nie L, Chen X. Structural and functional photoacoustic molecular tomography aided by emerging contrast agents. Chem Soc Rev. 2014; 43: 7132-70.
7. Luke G, Yeager D, Emelianov S. Biomedical Applications of Photoacoustic Imaging with Exogenous Contrast Agents. Ann Biomed Eng. 2012; 40: 422-37.
8. De La Zerda A, Zavaleta C, Keren S, Vaithilingam S, Bodapati S, Liu Z, et al. Carbon nanotubes as photoacoustic molecular imaging agents in living mice. Nat Nano. 2008; 3: 557-62.
9. Mallidi S, Larson T, Tam J, Joshi PP, Karpiouk A, Sokolov K, et al. Multiwavelength Photoacoustic Imaging and Plasmon Resonance Coupling of Gold Nanoparticles for Selective Detection of Cancer. Nano Lett. 2009; 9: 2825-31.
10. Gupta S, Chatni MR, Rao ALN, Vullev VI, Wang LV, Anvari B. Virus-mimicking nano-constructs as a contrast agent for near infrared photoacoustic imaging. Nanoscale. 2013; 5: 1772-6.
11. Lovell JF, Jin CS, Huynh E, Jin H, Kim C, Rubinstein JL, et al. Porphysome nanovesicles generated by porphyrin bilayers for use as multimodal biophotonic contrast agents. Nat Mater. 2011; 10: 324-32.
12. Huynh E, Lovell JF, Helfield BL, Jeon M, Kim C, Goertz DE, et al. Porphyrin Shell Microbubbles with Intrinsic Ultrasound and Photoacoustic Properties. J Am Chem Soc. 2012; 134: 16464-7.
13. Rieffel J, Chen F, Kim J, Chen G, Shao W, Shao S, et al. Hexamodal Imaging with Porphyrin-Phospholipid-Coated Upconversion Nanoparticles. Adv Mater. 2015; 27: 1785-90.
14. Rieffel J, Chitgupi U, Lovell JF. Recent Advances in Higher-Order, Multimodal, Biomedical Imaging Agents. Small. 2015; 11: 4445-61.
15. Huynh E, Leung BYC, Helfield BL, Shakiba M, Gandier J-A, Jin CS, et al. In situ conversion of porphyrin microbubbles to nanoparticles for multimodality imaging. Nat Nano. 2015; 10: 325-32.
16. Jeon M, Song W, Huynh E, Kim J, Kim J, Helfield BL, et al. Methylene blue microbubbles as a model dual-modality contrast agent for ultrasound and activatable photoacoustic imaging. J Biomed Opt. 2014; 19: 016005-10.
17. Luke GP, Myers JN, Emelianov SY, Sokolov KV. Sentinel Lymph Node Biopsy Revisited: Ultrasound-Guided Photoacoustic Detection of Micrometastases Using Molecularly Targeted Plasmonic Nanosensors. Cancer Res. 2014; 74: 5397-408.
18. Yang K, Zhu L, Nie L, Sun X, Cheng L, Wu C, et al. Visualization of protease activity in vivo using an activatable photo-acoustic imaging probe based on CuS nanoparticles. Theranostics. 2014; 4: 134-41.
19. Pu K, Shuhendler AJ, Jokerst JV, Mei J, Gambhir SS, Bao Z, et al. Semiconducting polymer nanoparticles as photoacoustic molecular imaging probes in living mice. Nat Nano. 2014; 9: 233-9.
20. Ke H, Erpelding TN, Jankovic L, Liu C, Wang LV. Performance characterization of an integrated ultrasound, photoacoustic, and thermoacoustic imaging system. J Biomed Opt. 2012; 17: 056010-6.
21. Kruger RA, Kuzmiak CM, Lam RB, Reinecke DR, Del Rio SP, Steed D. Dedicated 3D photoacoustic breast imaging. Med Phys. 2013; 40: 113301.
22. Jiang H. Diffuse optical tomography: principles and applications. CRC press; 2010.
23. Wang LV, Gao L. Photoacoustic Microscopy and Computed Tomography: From Bench to Bedside. Annu Rev Biomed Eng. 2014; 16: 155-85.
24. Bashkatov AN, Genina EA, Kochubey VI, Tuchin VV. Optical properties of human skin, subcutaneous and mucous tissues in the wavelength range from 400 to 2000 nm. J Phys D: Appl Phys. 2005; 38: 2543-55.
25. Homan K, Kim S, Chen YS, Wang B, Mallidi S, Emelianov S. Prospects of molecular photoacoustic imaging at 1064 nm wavelength. Opt Lett. 2010; 35: 2663-5.
26. Chen-Wei W, Thu-Mai N, Jinjun X, Arnal B, Wong EY, Pelivanov IM, et al. Real-time integrated photoacoustic and ultrasound (PAUS) imaging system to guide interventional procedures: ex vivo study. Ultrasonics, Ferroelectrics, and Frequency Control, IEEE Transactions on. 2015; 62: 319-28.

27. Ku G, Zhou M, Song S, Huang Q, Hazle J, Li C. Copper Sulfide Nanoparticles As a New Class of Photoacoustic Contrast Agent for Deep Tissue Imaging at 1064 nm. ACS Nano. 2012; 6: 7489-96.
28. Chen Y-S, Homan K, Xu D, Frey W, Emelianov S. Feasibility of Contrast-Enhanced Photoacoustic Liver Imaging at a Wavelength of 1064 nm. Biomedical Optics and 3-D Imaging. Miami, Florida: Optical Society of America; 2012: BM2B.7.
29. Hannah AS, VanderLaan D, Chen Y-S, Emelianov SY. Photoacoustic and ultrasound imaging using dual contrast perfluorocarbon nanodroplets triggered by laser pulses at 1064 nm. Biomed Opt Express. 2014; 5: 3042-52.
30. Kadish KM, Smith KM, Guilard R. The Porphyrin Handbook: Phthalocyanines: spectroscopic and electrochemical characterization. Elsevier; 2003.
31. Jiang J. Functional phthalocyanine molecular materials. Springer; 2010.
32. Zhang Y, Lovell JF. Porphyrins as theranostic agents from prehistoric to modern times. Theranostics. 2012; 2: 905-15.
33. Bottari G, de la Torre G, Guldi DM, Torres T. Covalent and noncovalent phthalocyanine− carbon nanostructure systems: synthesis, photoinduced electron transfer, and application to molecular photovoltaics. Chem Rev. 2010; 110: 6768-816.
34. Imahori H, Umeyama T, Kurotobi K, Takano Y. Self-assembling porphyrins and phthalocyanines for photoinduced charge separation and charge transport. Chem Comm. 2012; 48: 4032-45.
35. Bill NL, Trukhina O, Sessler JL, Torres T. Supramolecular electron transfer-based switching involving pyrrolic macrocycles. A new approach to sensor development? Chem Comm. 2015; 51: 7781-94.
36. Josefsen LB, Boyle RW. Unique diagnostic and therapeutic roles of porphyrins and phthalocyanines in photodynamic therapy, imaging and theranostics. Theranostics. 2012; 2: 916-66.
37. Machacek M, Cidlina A, Novakova V, Svec J, Rudolf E, Miletin M, et al. Far-Red-Absorbing Cationic Phthalocyanine Photosensitizers: Synthesis and Evaluation of the Photodynamic Anticancer Activity and the Mode of Cell Death Induction. J Med Chem. 2015; 58: 1736-49.
38. Komeda T, Katoh K, Yamashita M. Double-decker phthalocyanine complex: Scanning tunneling microscopy study of film formation and spin properties. Prog Surface Sci. 2014; 89: 127-60.
39. Rao SV. Phthalocyanines, Porphycenes, and Corroles: Nonlinear optical properties and ultrafast dynamics. SPIE Photonics Europe: International Society for Optics and Photonics; 2012: 84341B-10.
40. Sorokin AB. Phthalocyanine metal complexes in catalysis. Chem Rev. 2013; 113: 8152-91.
41. George NA, Jyotsna R, Lee ST, Aneeshkumar B, Thomas J, Nampoori V, et al. Photoacoustic spectrum of samarium phthalocyanine powder. Opt Mater. 2005; 27: 1593-5.
42. Attia ABE, Balasundaram G, Driessen W, Ntziachristos V, Olivo M. Phthalocyanine photosensitizers as contrast agents for in vivo photoacoustic tumor imaging. Biomed Opt Express. 2015; 6: 591-8.
43. Fukui T, Kishi M, Tomatsu F, Sasaguri D, Yuasa S. Phthalocyanine dye-containing contrast agent for photoacoustic imaging. United States Patent. US 20150037255A1; 2014.
44. Zhang Y, Jeon M, Rich LJ, Hong H, Geng J, Zhang Y, et al. Non-invasive multimodal functional imaging of the intestine with frozen micellar naphthalocyanines. Nat Nano. 2014; 9: 631-8.
45. Lee C, Kim J, Zhang Y, Jeon M, Liu C, Song L, et al. Dual-color photoacoustic lymph node imaging using nanoformulated naphthalocyanines. Biomaterials. 2015; 73: 142-8.
46. Furuyama T, Satoh K, Kushiya T, Kobayashi N. Design, synthesis, and properties of phthalocyanine complexes with main-group elements showing main absorption and fluorescence beyond 1000 nm. J Am Chem Soc. 2014; 136: 765-76.
47. Kobayashi N, Furuyama T, Satoh K. Rationally Designed Phthalocyanines Having Their Main Absorption Band beyond 1000 nm. J Am Chem Soc. 2011; 133: 19642-5.
48. Martin PC, Gouterman M, Pepich BV, Renzoni GE, Schindele DC. Effects of ligands, solvent, and variable sulfonation on dimer formation of aluminum and zinc phthalocyaninesulfonates. Inorg Chem. 1991; 30: 3305-9.
49. Erpelding TN, Garcia-Uribe A, Krumholz A, Ke H, Maslov K, Appleton C, et al. A dual-modality photoacoustic and ultrasound imaging system for noninvasive sentinel lymph node detection: preliminary clinical results. 2014. 894359.
50. Mbambisa G, Tau P, Antunes E, Nyokong T. Synthesis and electrochemical properties of purple manganese(III) and red titanium(IV) phthalocyanine complexes octa-substituted at non-peripheral positions with pentylthio groups. Polyhedron. 2007; 26: 5355-64.
51. Xu M, Wang LV. Universal back-projection algorithm for photoacoustic computed tomography. Phys Rev E. 2005; 71: 016706.